Supporting Information

$O3\text{-}Na_xMn_{1/3}Fe_{2/3}O_2$ as positive electrode material for Na-ion batteries: Structural Evolutions and Redox Mechanisms upon Na^+ (De)intercalation

B. Mortemard de Boisse,[a] J.-H. Cheng,[a,b] D. Carlier,*[a] M. Guignard,[a] C.-J. Pan,[b] S. Bordère,[a] D. Filimonov,[c] C. Drathen,[d] E. Suard,[e] B.-J. Hwang,[b,f] A. Wattiaux[a] and C. Delmas[a]

[a] CNRS, Université de Bordeaux, ICMCB, 33608 Pessac Cedex, France.

[b] Department of Chemical Engineering, National Taiwan University of Science and Technology (NTUST), Taipei 106, Taiwan.

[c] Chemistry Department, Lomonosov Moscow State University, Moscow 119991, Russia.

[d] ESRF, 6 rue Jules Horowitz BP 220, 38043 Grenoble, France.

[e] Institut Laue-Langevin, 71 Avenue des Martyrs, F-38000 Grenoble, France.

[f] National Synchrotron Radiation Research Center (NSRRC), Hsinchu 30076, Taiwan.

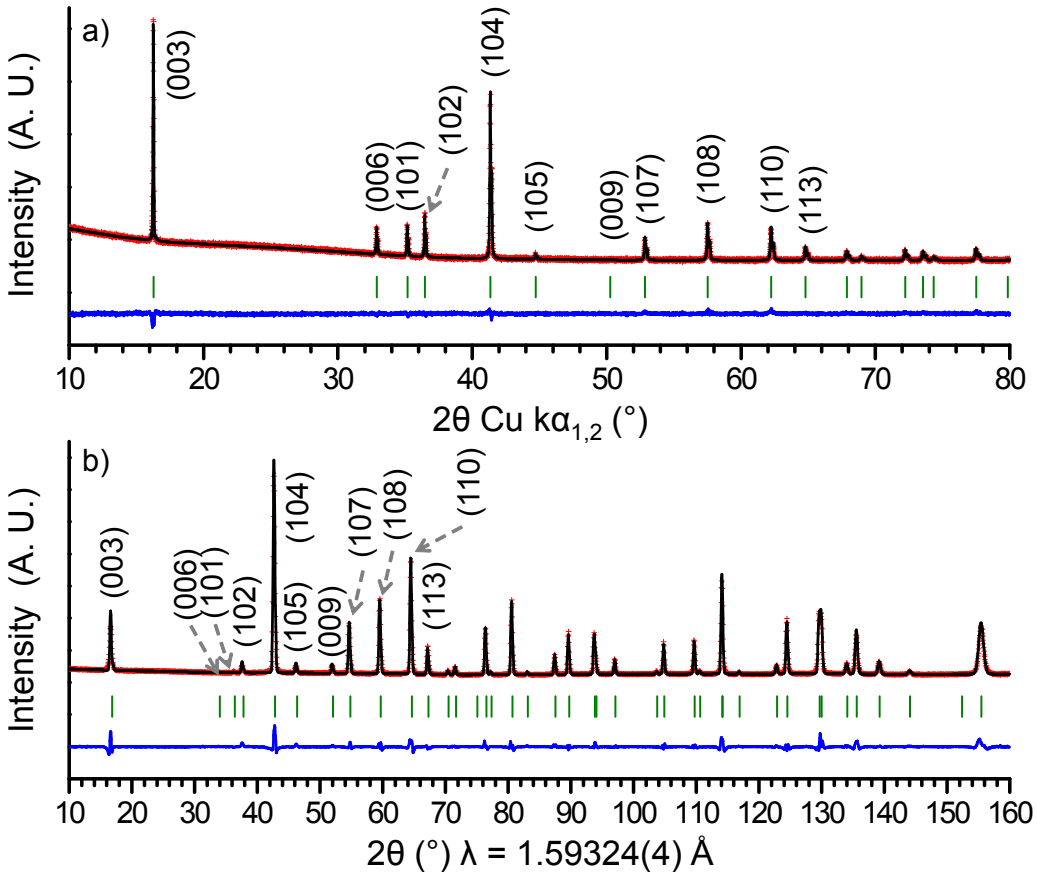

Figure S1. Observed and calculated (Rietveld method) (a) X-ray and (b) Neutron powder diffraction patterns for the "O3-$Na_{0.82}Mn_{1/3}Fe_{2/3}O_2$" starting phase at room temperature. Red crosses: experimental, black line: calculated, blue line: difference and green bars: Bragg positions.

		X-ray diffraction			Neutron diffraction	
Cell parameters (S.G.: **R-3m**)	$a_{hex.}$ (Å)	2.9804(1)				
	$c_{hex.}$ (Å)	16.3249(2)				
Wavelength (Å)		Cu k$\alpha_{1,2}$			1.59319(4)	
Atomic parameters:		x	y	z	Occ	ADP (Å²)
	Na (3b)	0	0	1/2	0.79(1)	1.54(3)
	Mn (3a)	0	0	0	0.32(1)	0.50(1)
	Fe (3a)	0	0	0	0.68(1)	
	O (6c)	0	0	0.269(1)	1	0.87(1)
R_{wp} (%)		2.07			6.75	
Global R_{wp} (%)		3.52				

Table S1: Structural parameters and reliability factors calculated from the combined refinement of the X-ray and Neutron powder diffraction patterns.

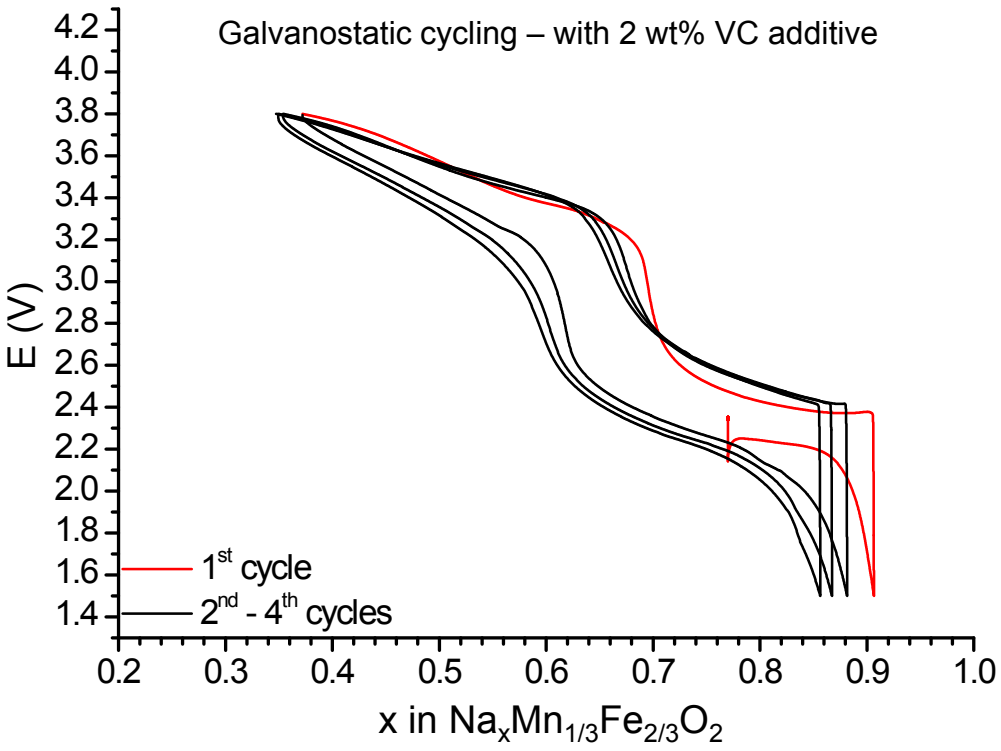

Figure S2. Galvanostatic cycling curve recorded at C/50 between 1.5 and 3.8 V with the VC electrolyte additive.

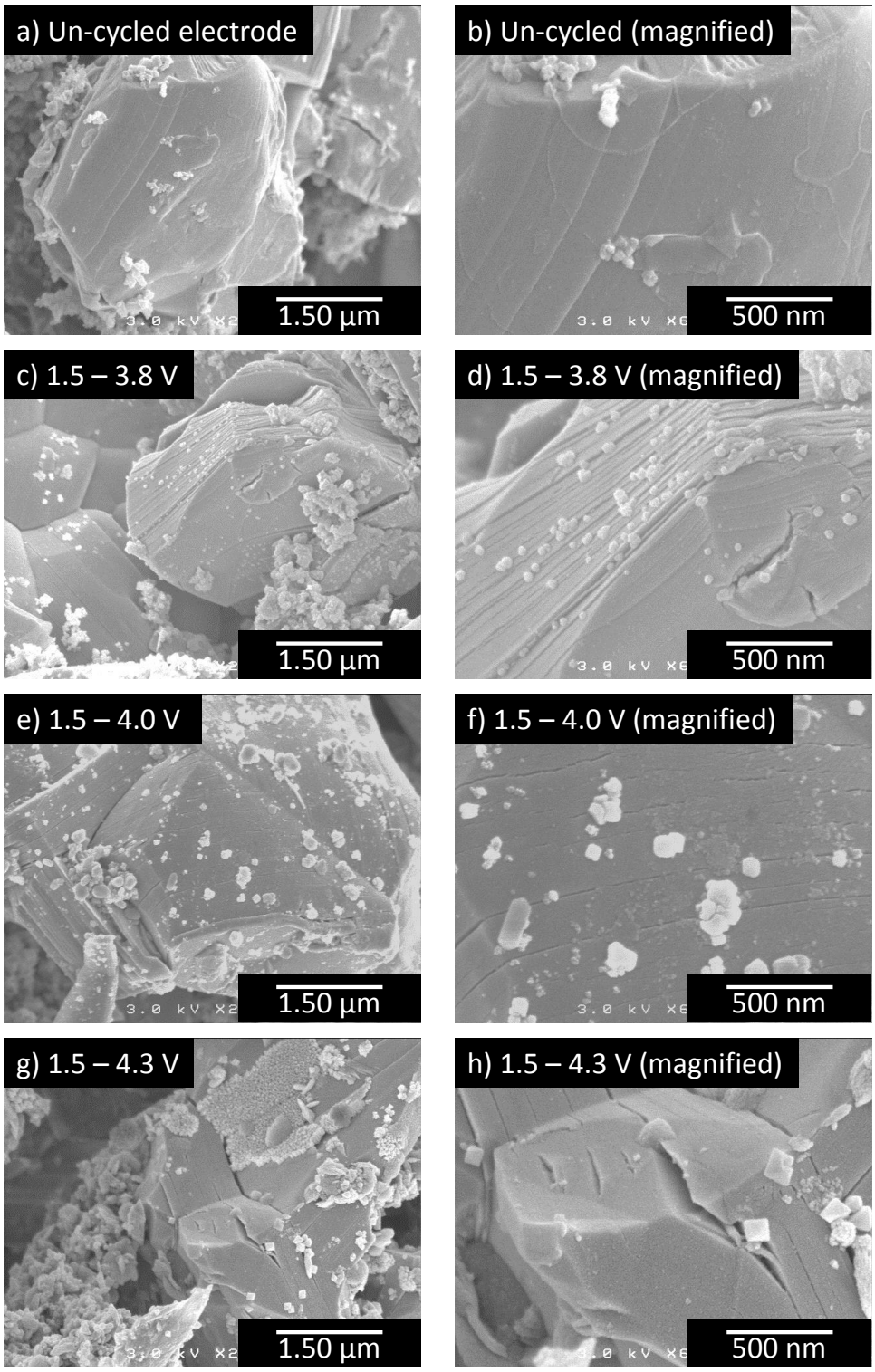

Figure S3. SEM micrographs of (a,b) an un-cycled electrode involving the O3-$Na_{0.77}Mn_{1/3}Fe_{2/3}O_2$ material and similar electrodes cycled 50 times (c,d) between 1.5 and 3.8 V, (e,f) between 1.5 and 4.0 V and (g,h) between 1.5 and 4.3 V.

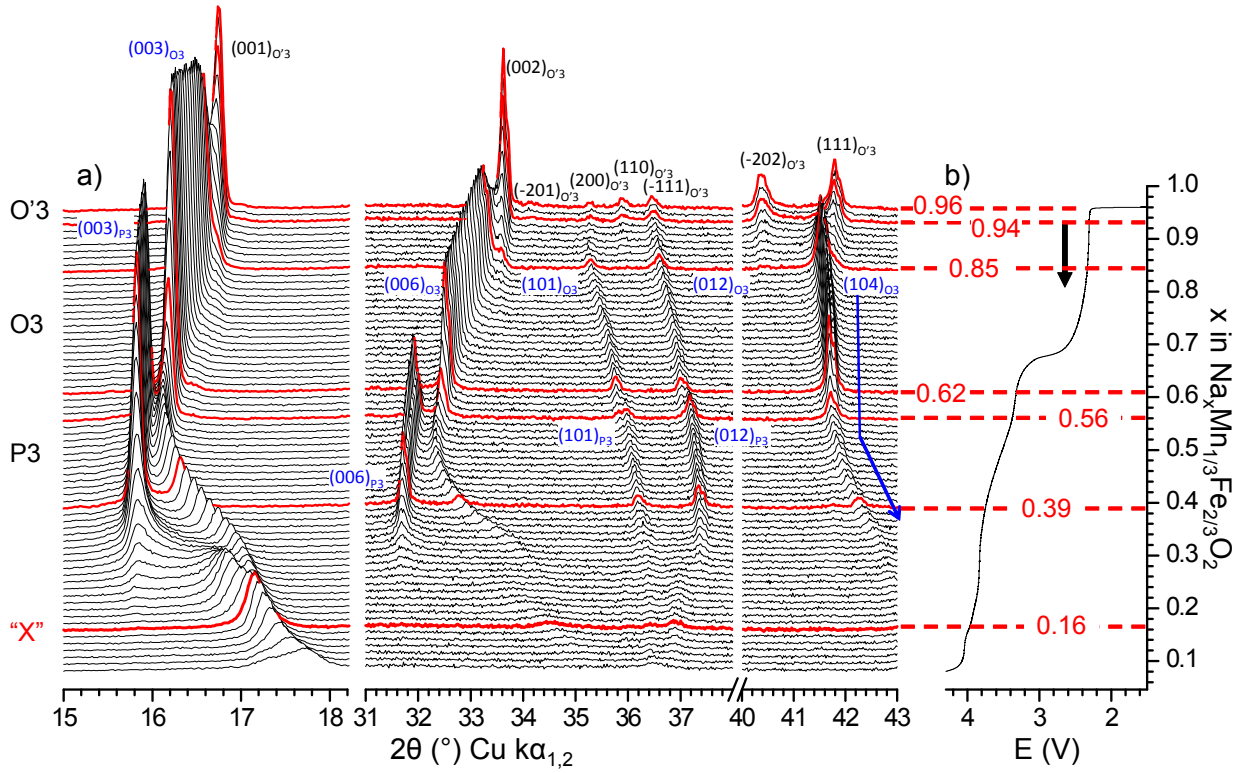

Figure S4. Inversed representation of Figure 5. (a) XRPD patterns recorded *in operando* during the charge of a $Na_xMn_{1/3}Fe_{2/3}O_2/NaPF_6$ in PC (1M)/Na cell along with (b) the corresponding galvanostatic curve. Blue Miller indexes: O3 and P3 phases. Black Miller indexes: O'3 phase.

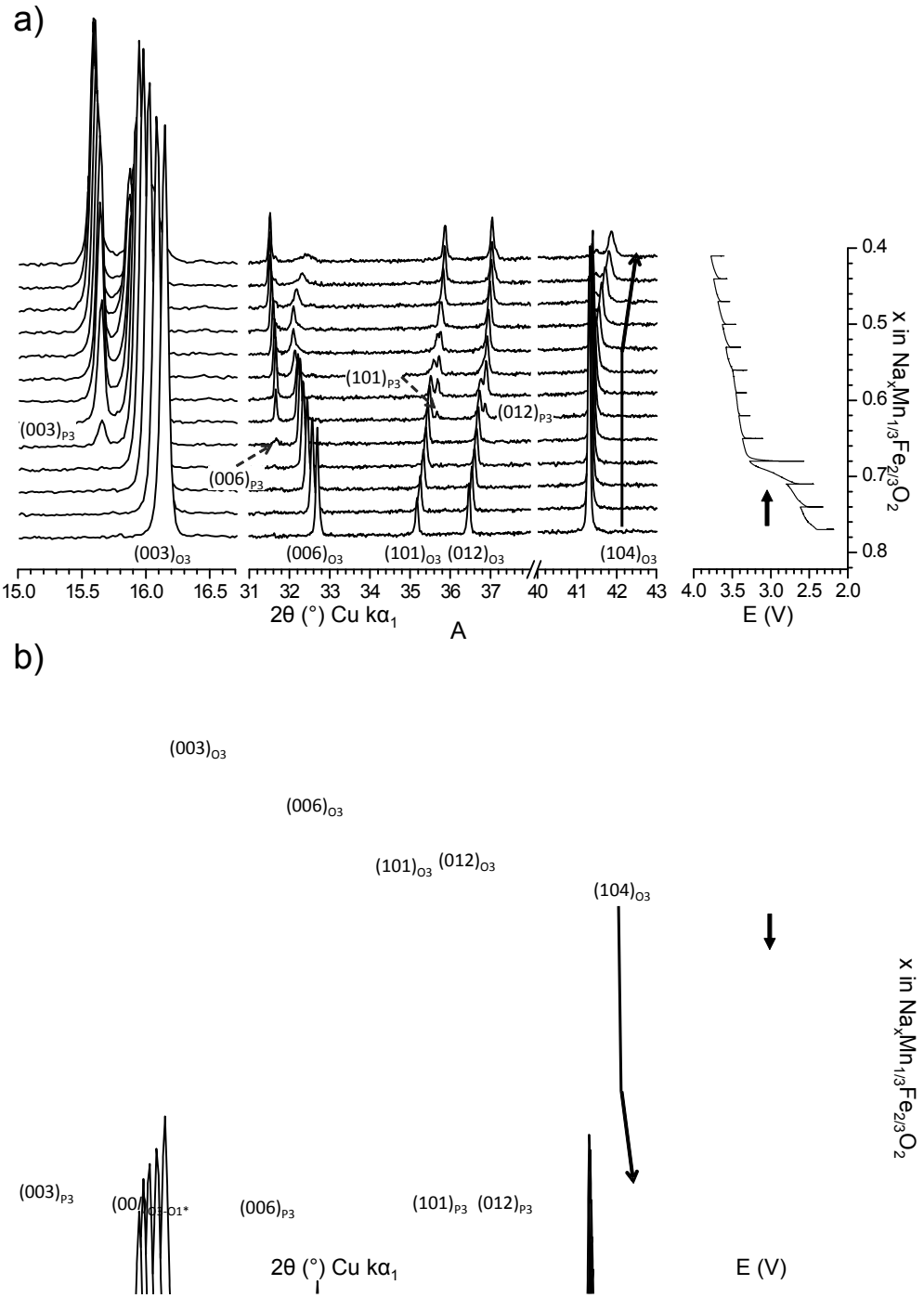

Figure S5. (left) XRPD patterns recorded *in* situ during the relaxation of a $Na_xMn_{1/3}Fe_{2/3}O_2$/$NaPF_6$ in PC (1M)/Na cell along with (right) the corresponding galvanostatic GITT curves.

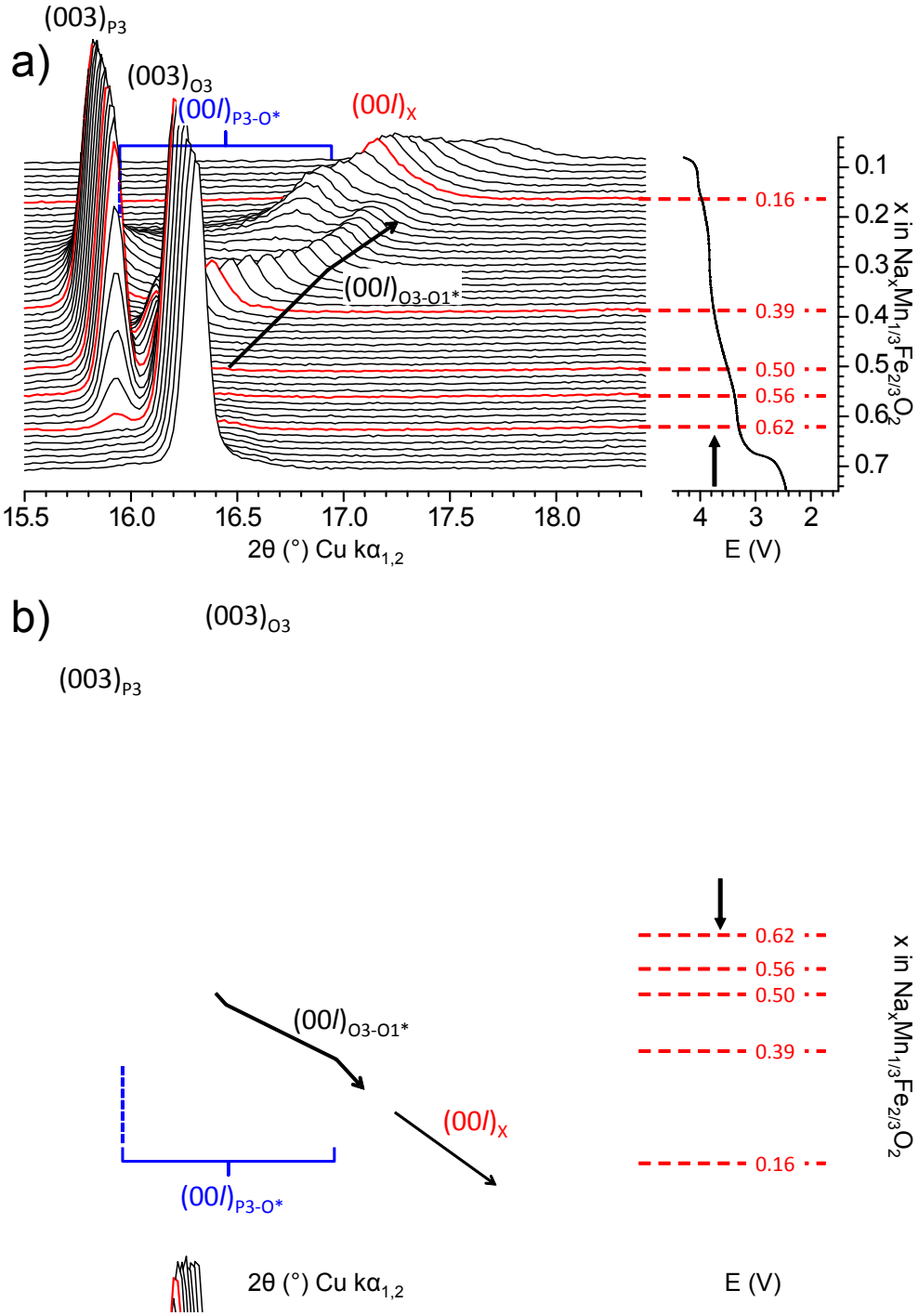

Figure S6. Magnifications in the $0.1 < x < 0.7$ region of the *operando* XRPD patterns recorded during the charge of the $Na_xMn_{1/3}Fe_{2/3}O_2/NaPF_6$ in PC (1M)/Na cell presented in Figures 5 and S3. The red lines highlight the limitations of the solid solutions and / or biphasic domains.

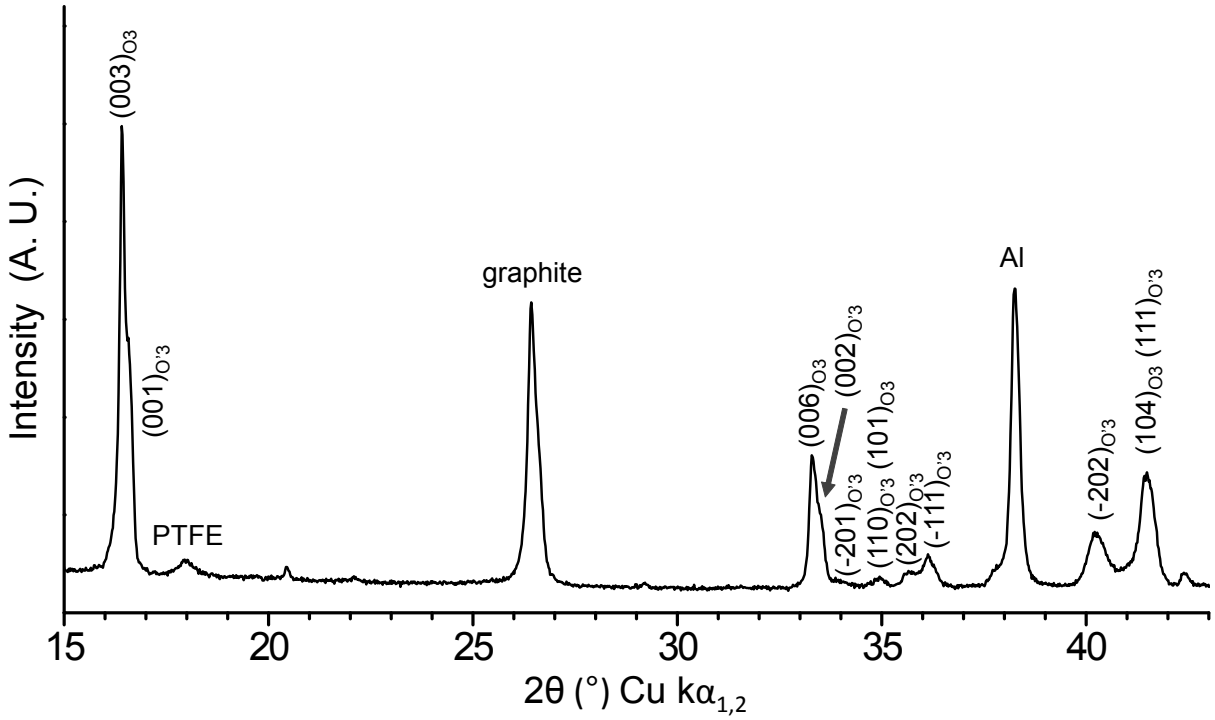

Figure S7. XRPD pattern of the electrode made of $Na_xMn_{1/3}Fe_{2/3}O_2$, carbon black and polytetrafluoroethylene (PTFE) recovered after charge to 4.3 V and discharge to 1.5 V. The aluminum diffraction peak arises from the sample holder.

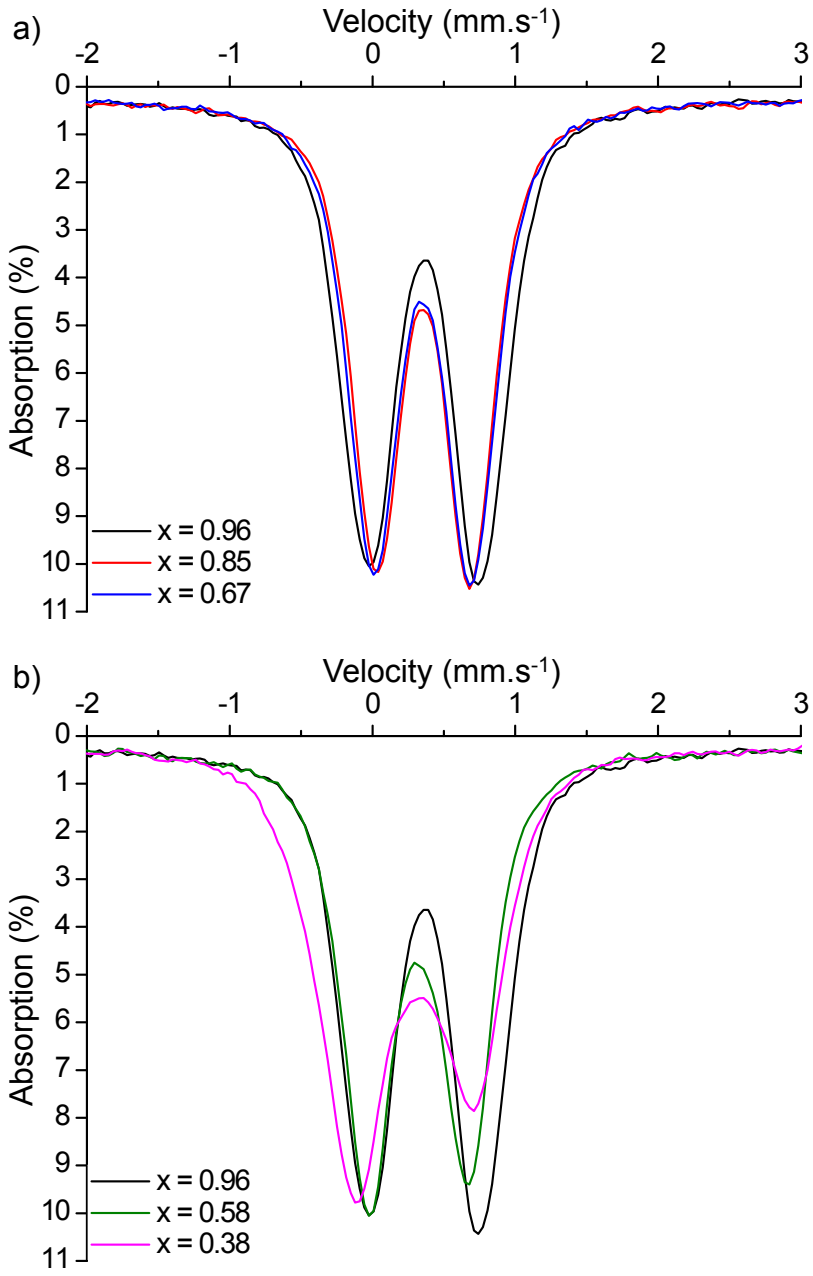

Figure S8. Superposition of the Mössbauer spectra corresponding to (a) the $x = 0.96$ (black line), $x = 0.86$ (red line) and $x = 0.67$ (blue line) compositions and to (b) the $x = 0.96$ (black line), $x = 0.58$ (green line) and $x = 0.38$ (pink line) compositions.